ON SURFACE ENERGY EFFECTS IN COMPOSITE IMPREGNATION AND CONSOLIDATION

Marco Connor, Staffan Toll and Jan-Anders E. Månson*

Laboratoire de Technologie des Composites et Polymères
Ecole Polytechnique Fédérale de Lausanne
CH-1015 Lausanne, Switzerland

Macroscopic capillary pressure and microscopic inter-particle forces due to surface tension are examined. A general equation for the capillary pressure during impregnation is derived and subsequently specialised to particular processes. For fibre composites, the capillary pressure can be of the order of $\pm 10^4$ Pa, the sign depending on the contact angle between solid and liquid. Next, the attractive and repulsive forces between particles connected by liquid droplets are analysed by two different model geometries. At contact angles between $\pi/2$ and π, an equilibrium particle separation distance is obtained in the absence of applied force. At lower contact angles, spontaneous impregnation can be achieved. The effect of capillary action on impregnation rate may be significant if applied pressures are small (e.g. filament winding) but negligible at applied pressures greater than ~100 kPa (e.g. compression moulding). The topology and concentration of voids may, however, be greatly influenced by surface energies.

1 INTRODUCTION

Composite impregnation and consolidation processes usually involve the flow of a liquid matrix into an assembly of closely spaced particles of the order of 10 μm size (e.g. fibres). The liquid must flow through long and narrow channels and wet a large surface area of particles. In such conditions the surface energies of the various phases are likely to play an important role. Surface energy effects can be described on at least two levels: the macroscopic level, where they appear as a capillary pressure, and the micromechanical level, where they appear as forces acting between individual particles. This paper addresses both.

Capillary pressure, P_c, is defined as

$$P_c = -\frac{dE}{dV} \tag{1}$$

where E is the total surface and interfacial energy in the volume V. The capillary pressure determines whether spontaneous impregnation can occur: if the total amount of surface energy decreases upon impregnation the capillary pressure will be negative and impregnation (decrease of volume) will tend to be spontaneous; if the energy increases, the system resists impregnation and impregnation will take place only under externally applied pressure.

The capillary force between particles connected by a resin droplet is defined similarly

$$F_c = \frac{dE}{da} \tag{2}$$

where a is the distance between the particles. The capillary forces between particles are of course the microscale origin of the capillary pressure.

* To whom correspondence should be addressed

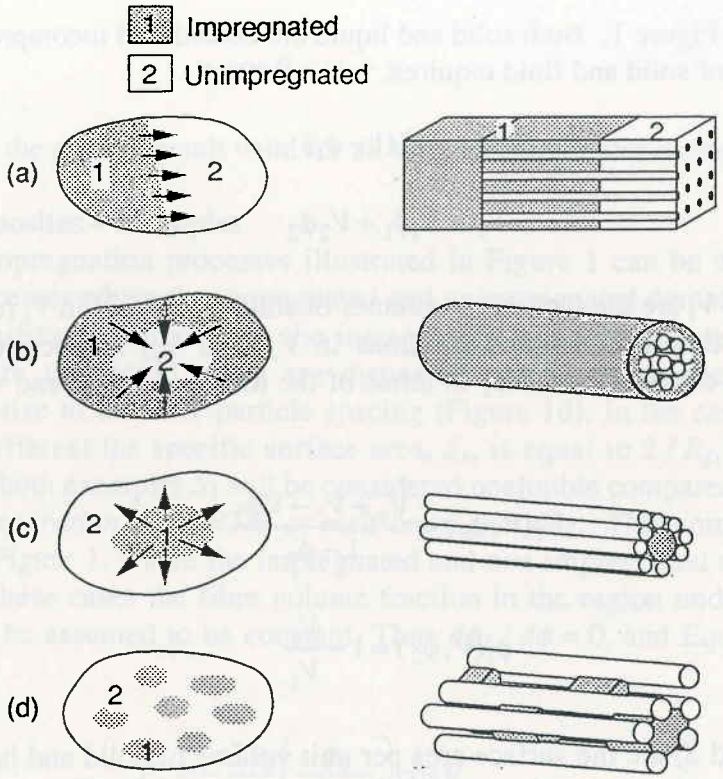

***Figure 1**: Different impregnation situations: (a) advancing front (e.g. RTM); (b) radial impregnation of a fibre bundle; (c) commingled fibres; and (d) liquid dispersed among the solid particles (e.g. powder impregnation).*

Figure 1 illustrates the most common impregnation or consolidation situations. Figure 1a shows the case of resin transfer moulding (RTM), melt impregnation or infiltration; Figure 1b shows radial impregnation of a fibre bundle [1]; Figure 1c shows impregnation by commingled resin fibres [2]; and Figure 1d shows the case of a liquid dispersed among the solid particles, e.g. consolidation of powder impregnated tows [3]. One can further distinguish low-pressure techniques, using applied pressures of the order of 10^5 Pa, (e.g. vacuum bagging, filament winding) from higher-pressure techniques using the order of 10^6–10^7 Pa, usually for high viscosity thermoplastic matrices (e.g. autoclave forming, compression moulding). Capillary effects are more likely to be significant when applied pressures are low.

In this paper, a general expression for the capillary pressure is derived based on Equation (1), allowing for a completely general pore geometry and a solids volume fraction that may vary during impregnation. Specialisation is then made to the various cases in Figure 1. Next, the capillary forces between particles connected by liquid droplets are examined by considering two different geometries: parallel square-section fibres and parallel plates.

2 CAPILLARY PRESSURE

2.1 General theory

Consider a volume V divided into two types of subdomains: the impregnated volume, V_1, consisting of solid and liquid, and the unimpregnated volume V_2, consisting of solid

and void, see Figure 1. Both solid and liquid are considered incompressible. Now mass conservation of solid and fluid requires:

$$V_l = V_1(1-\phi_1) \tag{3}$$

$$V_s = V_1\phi_1 + V_2\phi_2 \tag{4}$$

where V_s and V_l are the (constant) volumes of solid and liquid in V, respectively, and ϕ_1 and ϕ_2 are the solid volume fractions in V_1 and V_2, respectively. This can be rearranged to express V_1 and ϕ_1 in terms of the total volume V and volume fraction ϕ_2 only:

$$V_1(V,\phi_2) = \frac{V_s + V_l - V\phi_2}{1-\phi_2} \tag{5}$$

$$\phi_1(V,\phi_2) = 1 - \frac{V_l}{V_1} \tag{6}$$

If S_s and S_l are the surface area per unit volume of solid and liquid, respectively, then the surface energy can be expressed as

$$E = S_s\left[\phi_1 V_1 \gamma_{sl} + \phi_2 V_2 \gamma_s\right] + S_l V_1 \gamma_l \tag{7}$$

where γ_l, γ_s, and γ_{sl} are the surface energy per unit area of liquid, solid, and solid-liquid interface, respectively. By introducing Equations 5 and 6 into (7), E can be written as a function of V and ϕ_2:

$$E = \frac{1}{1-\phi_2}(V_s+V_l)(S_s\gamma_{sl} + S_l\gamma_l) - \frac{\phi_2}{1-\phi_2}(V_s+V_l)S_s\gamma_s + \frac{V\phi_2}{1-\phi_2}(S_s\gamma_s + S_l\gamma_l - S_s\gamma_{sl}) - V_l S_s\gamma_s \tag{8}$$

Allowing for ϕ_2 (the solids volume fraction in the regions under impregnation) to vary during impregnation, the capillary pressure according to Equation 1 can be expressed as

$$-P_c = \frac{dE}{dV} = \frac{\partial E}{\partial V} + \frac{\partial E}{\partial \phi_2}\frac{d\phi_2}{dV} \tag{9}$$

which, together with Equation 8, gives the final result:

$$P_c = -\gamma_l(S_s\cos\theta + S_l)\left(\frac{\phi_2}{1-\phi_2} - \frac{\phi\phi_v}{(1-\phi_2)^2}\frac{d\phi_2}{d\phi}\right) \tag{10}$$

where ϕ_v is the void volume fraction and θ is the contact angle, related to the surface energies through the Young Equation

$$\gamma_l \cos\theta = \gamma_s - \gamma_{sl} \tag{11}$$

Equation 10 is the general result valid for all the processes under consideration here.

2.2 Fibre composites – examples

The specific impregnation processes illustrated in Figure 1 can be divided into two classes: (i) processes where the impregnated and unimpregnated domains are separated on a scale significantly larger than the inter-particle spacing (Figure 1a–c), and (ii) processes where the liquid pools are dispersed among the particles in domains comparable in size to the inter-particle spacing (Figure 1d). In the case of cylindrical reinforcement (fibres) the specific surface area, S_s, is equal to $2 / R_f$, where R_f is the fibre radius. In both examples S_l will be considered negligible compared to S_s.

(i) Full separation (e.g. RTM or melt impregnation). This comprises cases (a) through (c) in Figure 1, where the impregnated and non-impregnated regions are fully separated. In these cases the fibre volume fraction in the region under impregnation (region 2) will be assumed to be constant. Thus $d\phi_2 / d\phi = 0$, and Equation 10 can be written as

$$P_c = -\frac{2\gamma_l}{R_f}\left(\frac{\phi_2}{1-\phi_2}\right)\cos\theta \tag{12}$$

This equation is identical to the result proposed by Ahn et al. [4] for resin transfer moulding.

(ii) Full dispersion (e.g. powder impregnation). Since the liquid phase is fully dispersed among the solid particles, the fibre volume fraction is homogeneous, so $\phi_2 = \phi$, and $d\phi_2 / d\phi = 1$. Equation 10 can thus be written as

$$P_c = -\frac{2\gamma_l}{R_f}\left(\frac{\phi}{1-\phi}\right)^2\left(\frac{1-\phi}{\phi}\right)_{Final}\cos\theta \tag{13}$$

This is the same expression as proposed in [5] for powder impregnated composites. It should be noted that our neglect of the free liquid surface restricts Equation 13 to the final stages of an impregnation process. In order to capture the early stages it would be necessary to model the free liquid surface area per unit volume of liquid S_l, which unlike S_s is a function of V. This requires a more detailed description on the particle level, and is thus left for the next section.

Equations 12 and 13 are plotted as a function of ϕ_2 in Figure 2 using parameters typical of a fibre-resin system, i.e. $\gamma_l = 4.0 \times 10^{-2}$ Pa·m, $\theta = \pi/6$, $R_f = 3.5$ μm, and the final fibre content, $\phi_{final} = 0.65$. In the *fully separated* case (Equation 12), the fibre volume fraction does not vary during impregnation. The solid line therefore gives the capillary pressure for all volume fractions. By contrast, in the *fully dispersed* case (Equation 13), P_c evolves during the impregnation of one system; this evolution (dashed line) is determined by the fibre volume fraction at the fully consolidated state, ϕ_{final}, where Equations 12 and 13 become equivalent.

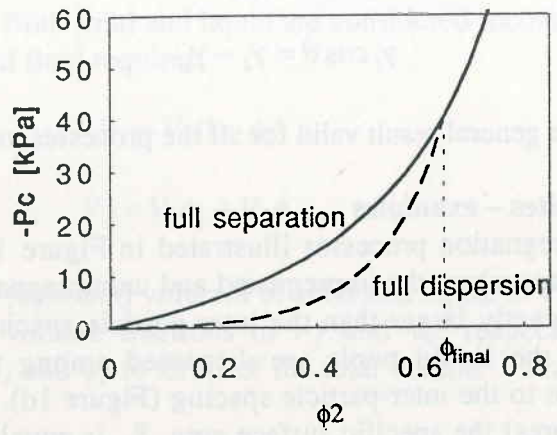

Figure 2: Capillary pressure as a function of the fibre volume fraction: the full separation case correspond to Eq. 12 and the full dispersion one to Eq. 13.

3 CAPILLARY INTER-PARTICLE FORCES

We have seen that the macroscopic effects of surface energy can be evaluated based on average geometrical quantities such as volume fractions and surface area per unit volume of the various phases. An understanding of the capillary forces acting on the micromechanical level requires, however, a detailed description of particle shape and arrangement. Here we shall focus on the situation in Figure 1d, where the liquid is dispersed as small droplets between the solid particles. This situation may arise in thermoplastic powder impregnation, where the liquid droplets are formed by the melting of powder grains, or in resin transfer moulding or melt impregnation, where droplets may form by splitting of a flow front [6]. The liquid droplets will tend to adopt a shape which minimises the surface energy. If a droplet makes contact with two or more particles, it may either repel or attract the particles depending on the various surface energies. A value of the particle spacing may also exist for which the capillary force vanishes. This then corresponds to an equilibrium state to which the system tends in the absence of applied pressure. Capturing this effect requires geometric modelling of S_l and is thus missed by our previous result (Equations 12 and 13), which neglects S_l. Here we shall merely illustrate the nature of the capillary microforces and show when an equilibrium state exists. Many different geometries can be envisaged. Two have been chosen here based on analytical and experimental feasibility: a droplet in contact with, in the first case, two parallel square-section fibres, and, in the second case, two parallel plates; the former has a simple analytical solution, whereas the latter requires a numerical solution but can be experimentally realised.

3.1 Droplet in contact with two parallel square-section fibres

A good description, at the qualitative level, is afforded by the idealised geometry depicted in Figure 3, where two cases are represented: $\theta < \pi/2$ and $\theta > \pi/2$. The contact angle is of course bounded by $0 \le \theta \le \pi$. To calculate the capillary inter-particle force, the following assumptions are made: both liquid and solid are incompressible; the drop volume, V, is constant, $dV / da = 0$; the contact angle, θ, is constant, $d\theta / da = 0$; and the curved liquid surface is cylindrical. The capillary force, F_c, is taken positive when the fibres are pulled together.

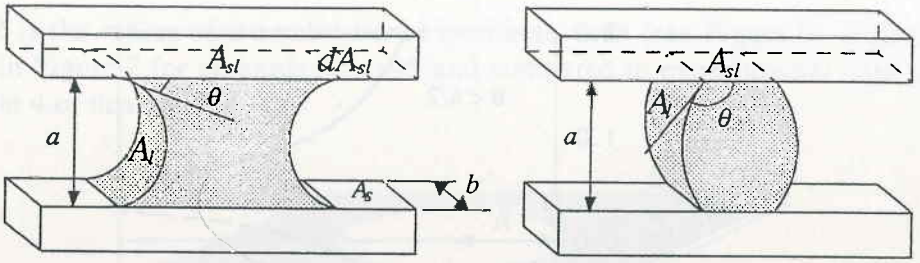

(a) $\theta < \pi/2$ (b) $\theta > \pi/2$

***Figure 3**: A liquid droplet bridging two parallel square section fibres: (a) $\theta < \pi/2$, and (b) $\theta > \pi/2$.*

Statically, the work, $F_c\,da$, required to move the fibres a distance, da, apart is equal to the variation of the surface energy, dE, of the system,

$$F_c da = dE = \gamma_l dA_l + \gamma_s dA_s + \gamma_{sl} dA_{sl} \tag{14}$$

Based on the geometry represented in Figure 3 the various surface area variations, dA, can be related to the variation of distance, da, between the fibres as,

$$dA_l = 2b\frac{\left(\frac{\pi}{2}-\theta\right)}{\cos\theta}\cdot da \tag{15}$$

and

$$dA_{sl} = -dA_s = \left[-2\frac{V}{a^2} + b\left(\frac{\left(\frac{\pi}{2}-\theta\right)}{\cos^2\theta} - \tan\theta\right)\right]\cdot da \tag{16}$$

Introducing Equations 15 and 16 into Equation 14 and using the Young equation (Equation 11) allows the capillary force, F_c, to be expressed as a function of the distance between the two fibres, a, as,

$$F_c(a,\theta) = \gamma_l\left(b\frac{\left(\frac{\pi}{2}-\theta\right)}{\cos\theta} + b\sin\theta + 2\frac{V}{a^2}\cos\theta\right) \tag{17}$$

which is plotted in Figure 4 for an angle, θ, smaller and greater than zero, respectively. For angles smaller than $\pi/2$, the force is always attractive ($F_c>0$) and increases as the fibres are pulled together. For angles greater than $\pi/2$, however, the fibres are first driven closer together, until they reach an equilibrium distance, a_0, at which point the capillary force, F_c, is zero. Any attempt to drive them closer would require the application of an external force.

The equilibrium distance, a_0, can be found by setting the force, F_c, in Equation 17 to zero. This can be written as a dimensionless distance, $a_0^* = a_0\sqrt{b/V}$ as

$$a_0^* = \frac{2\cos\theta}{\sqrt{2\theta - \pi - \sin 2\theta}} \tag{18}$$

which is defined for angles greater than $\pi/2$ only, and is plotted in Figure 5.

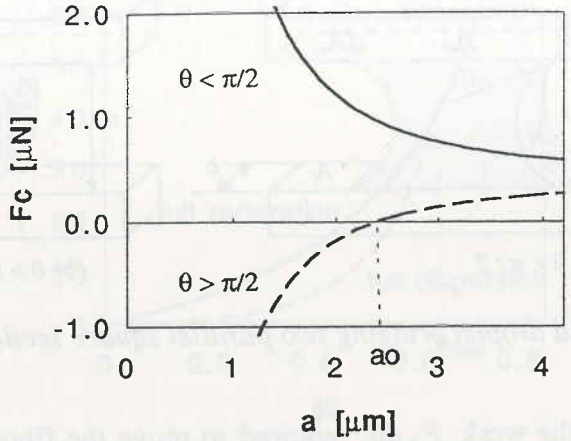

Figure 4: Capillary force as a function of the distance between fibres (Eq. 17) with $\gamma_l = 4.0x10^{-2}$ Pa.m, b = 5 μm, V = 10^3 $μm^3$, θ = 87.7°(solid line), and θ = 91.7°(dashed line).

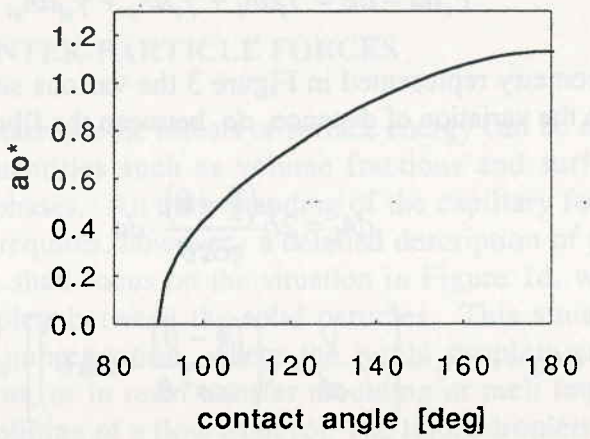

Figure 5: Equilibrium distance, a_0, as a function of the contact angle (Eq. 18).*

3.2 Droplet in contact with two parallel plates

The geometry depicted in Figure 6, an axisymmetric droplet of fluid generated by the rotation of a circular arc, in contact with two parallel plates is relatively close to the geometry shown in Figure 9, yet allowing a fairly simple derivation. Furthermore, it can readily be reproduced experimentally. Following the same procedure as in section 3.1, an expression for the force as a function of the distance between the two plates and the contact angle can be derived from Equation 14:

$$F_c(a,\theta) = 2\pi\gamma_l\left[R + a\frac{dR}{da} + \frac{a}{2}\tan\theta + \frac{a}{2\cos^2\theta}\left(\theta - \frac{\pi}{2}\right) - 2R\,\frac{dR}{da}\cos\theta\right] \qquad (19)$$

where $$\frac{dR}{da} = \frac{1}{2}\frac{\frac{a}{8}\Phi^2 - \frac{a}{2}\Theta + \frac{V}{a^2\pi}}{\sqrt{\frac{a^2}{16}\Phi^2 - \frac{a^2}{4}\Theta + \frac{V}{a\pi}}} - \frac{\Phi}{4}$$

with $$\Phi = \tan\theta + \frac{\left(\theta - \frac{\pi}{2}\right)}{\cos^2\theta}$$

and $$\Theta = \frac{1}{\cos^2\theta} + \frac{\tan\theta}{\cos^2\theta}\left(\theta - \frac{\pi}{2}\right) - \frac{1}{3}$$

where R is the radius of the solid-liquid interfacial area (see Figure 6). Equation 19 is plotted in Figure 7 for an angle $\theta = 145°$and compared to experimental data presented in section 4 of this paper.

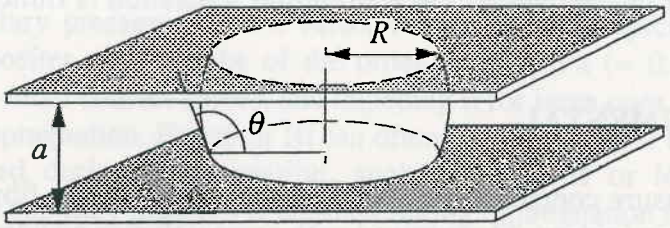

Figure 6: Axi-symmetric droplet bridging two parallel plates.

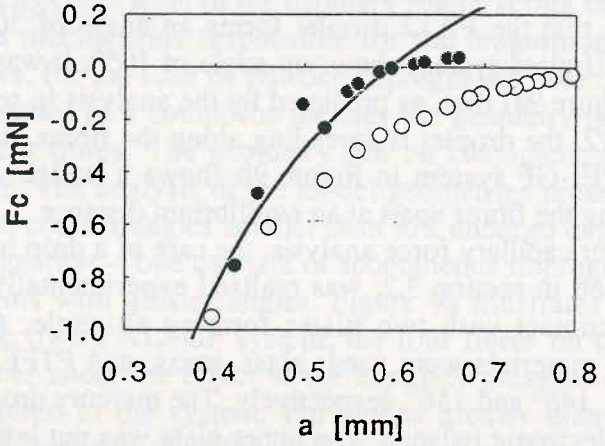

***Figure 7**: Capillary force as a function of the distance between plates. The solid line is obtained with Eq. 19, the circles are experimental data obtained by lowering (white) then raising (black) the upper plate.*

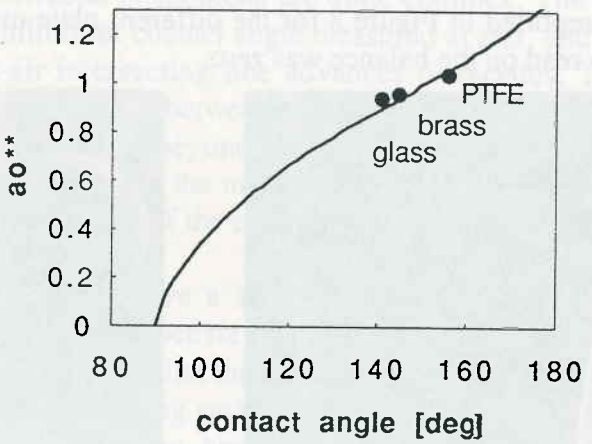

***Figure 8**: Equilibrium distance, a_0**, as a function of the contact angle . The solid line is obtained by numerically solving $F_c = 0$ in Eq. 19. The circles are experimental data.*

It can be seen that the force is positive (attractive) when the plates are some distance apart. As they are brought together the force falls, reaching zero at $a_0 = 680$ µm, the equilibrium condition, then becoming negative (repulsive). In order to obtain the dimensionless equilibrium separation, $a_0{**}=a_0 \cdot V^{-1/3}$, as a function of the contact angle,

the force value in Equation 19 is put to zero and the resulting relationship is evaluated numerically. The result is shown in Figure 8 and compared to experimental data. It can be seen that, as found in section 3.1 for the square-section fibre geometry, for all contact angle values lower than $\pi/2$ the equilibrium plate separation distance is zero, while for higher contact angles the equilibrium separation is finite and increases with contact angle.

4 EXPERIMENTAL

In order to measure contact angles between the resin and the fibres and observe the formation of resin bridges, fibres mixed with some polymer powder were heated above the softening point (or melting point for semi-crystalline resins) for five minutes, then cooled in air. Figure 9 shows SEM micrographs of polyamide 12 (PA12) and poly(etherimide) (PEI) on glass fibres (GF) obtained at 220°C and 280°C, respectively. It can be seen that the PA12 droplet forms an angle of 30° with the fibre surface, whereas the PEI/glass system shows an angle of 105°. It was observed for the PA-12-GF system (Figure 9a) that, as predicted by the analysis in section 3 for contact angles smaller than $\pi/2$, the droplet is spreading along the fibres, drawing them together. By contrast, the PEI-GF system in Figure 9b shows a bridge which did not spread and which is holding the fibres apart at an equilibrium distance.

To test our capillary force analysis, the case of a drop in contact with two parallel plates, examined in section 3.2, was realised experimentally. A mercury droplet was brought into contact with two plates forming an angle, θ, with the liquid. Three different plate materials were used: glass, brass, and PTFE plates producing contact angles of 141°, 145° and 156°, respectively. The mercury drop and the lower plate were placed on an electronic balance. The upper plate was put into contact with the droplet, then lowered and successively raised with a micrometric screw. The magnitude of the capillary force was directly read on the balance for different plate separations, a. Figure 7 reports the values of the measured force as a function of distance, a, for a contact angle of 145° (brass plate) and compares them to Equation 19. The equilibrium distance a_0** reported in Figure 8 for the different plate materials was obtained when the force value read on the balance was zero.

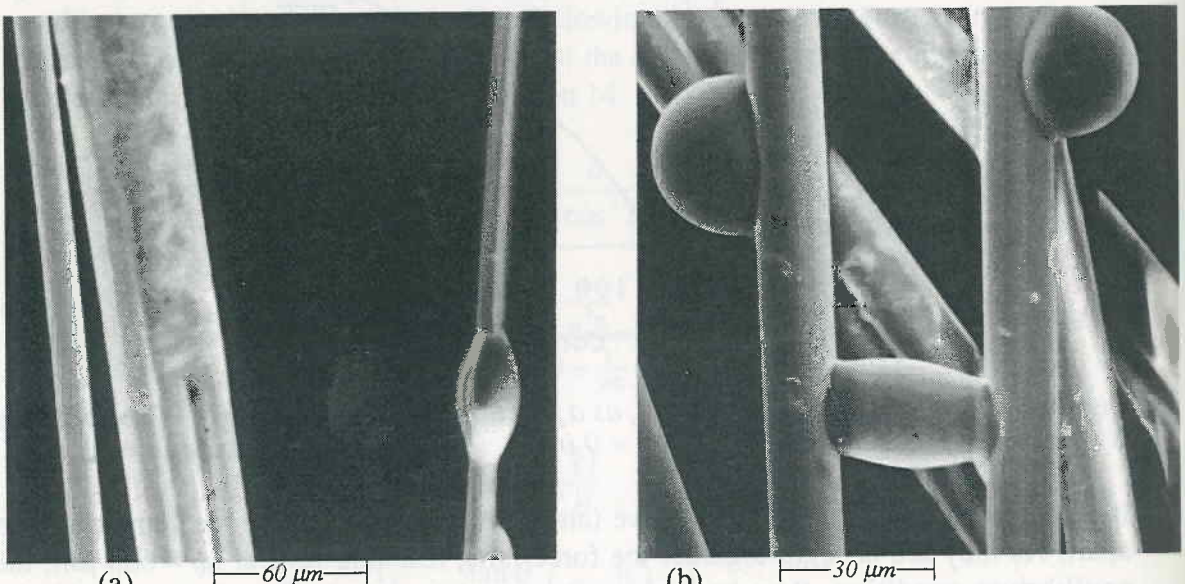

***Figure 9**: Molten resin droplet bridging glass fibres: (a) PA12, θ = 30°, and (b) PEI, θ = 105°.*

5 DISCUSSION

The calculation of the capillary pressure, P_c, (Eq. 10, 12 and 13) allows the magnitude of the surface energy effects to be directly compared to other processing parameters, such as the mechanical pressure applied during manufacturing of fibre reinforced laminates. Capillary pressure takes a value, for parameters typical of carbon fibre reinforced composites, that can be of the order of $\pm 10^4$ Pa (= 0.1 bar), enhancing impregnation for small contact angles, and impeding it for large ones. Depending on the mechanism of impregnation, Equation 10 can often be simplified. If the fibre bed is not being compressed during impregnation, such as in RTM or low pressure melt impregnation, the capillary pressure is constant during impregnation and proportional to $\phi_2 / (1-\phi_2)$, where ϕ_2 is the fibre volume fraction in the "dry" fibre bed (Equation 12). If, on the other hand, impregnation is accompanied by a compression of the fibre bed, the capillary pressure increases during impregnation (Equation 13).

A study at the microscopic level of the capillary forces acting between individual particles elucidates the mechanisms responsible for the magnitude of the capillary pressure. Figure 9 shows, for the case of powder impregnated fibres, how the surface energy of the various phases of a composite dictates the geometry of the resin bridge formed between adjacent fibres. The geometry can be characterised by the contact angle, θ, at the interface. The analysis of the model geometries presented in section 3 shows that systems with contact angles smaller than $\pi/2$ undergo capillary forces that enhance the melt impregnation —one can talk of spontaneous impregnation— whereas they impede it in systems with greater angles. Figure 9a illustrates the spontaneous impregnation undergone by a PA12-GF system; the four fibres on the left hand-side have been pulled together under the effect of the capillary pressure only, no external forces having been applied to the system. For angles greater than $\pi/2$, there is an equilibrium distance, a_0, between the fibres which corresponds to a minimum of the energy of the system (see Figure 4b).

It must be noted that the analyses in sections 3.1 and 3.2 describe a simplified situation with constant interfacial energies and contact angle, and simplified geometries. In reality, interfacial phenomena are quite complex. The dynamic contact angle differs from the equilibrium contact angle measured at rest, and will be different whether the solid-liquid-air intersecting line advances or recedes. This explains the existence of a hysteresis, in Figure 7, between the advancing and receding forces [7, 8]. Such considerations, however, lie beyond the scope of this work. The agreement between the experimental values and the model, in Figures 7 and 8, is acceptable and already affords a fair understanding of the effects of the surface energies in connection with composite manufacturing.

The capillary pressure can have a significant influence on the impregnation quality and rate in low pressure processes, such as bagging technique or filament winding. Bascom et al. [9] observed that the void content in filament wound rings was markedly reduced when resins showing small contact angles with the fibres were used. In thermoplastic composites processing, however, mechanical pressures of the order of 10^5–10^7 Pa are usually applied, such as in autoclave forming or compression moulding, for instance. In this situation the driving force from surface energy effects will be small compared to that arising from the externally applied pressure. This is not to imply that surface energy effects are unimportant, however: in many systems a quantity of air may be entrapped during wet-out, and this will remain in the part after processing. This may affect the composite properties as studied by Kohn et al. [10] who measured a linear inverse relation between the interlaminar shear strength and the microvoid content. The

topology of any voids remaining in the composite will be critical to their effect on mechanical properties, as illustrated schematically in Figure 10. As suggested by Szymanski [11], under favourable wetting conditions the area of the solid/air interface will be minimised and any entrapped void spaces will tend to coalesce in regions away from the fibres, as shown in Figure 10a, so that the effect of such regions on load transmission near to the fibre/matrix interface will be minimised. Under poor wetting conditions, however, with a large contact angle there is no driving force for the system to expel air and the void space will actually be concentrated adjacent to the surface of the fibres, as shown in Figure 10b, where its effects on mechanical properties will be greatest.

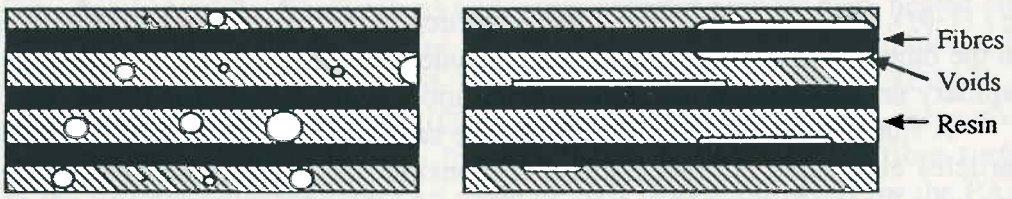

***Figure 10**: Schematic of the topology of the voids in a laminate as a function of the contact angle, (a) $\theta < \pi/2$ and (b) $\theta > \pi/2$.*

6 CONCLUSION

A general expression was derived for the capillary pressure during impregnation of a porous solid by a liquid. For impregnation of a fibre bed by a resin, the magnitude of the capillary pressure can be of the order of $\pm 10^4$ Pa, the sign of which depends on the value of the contact angle. In the case of small contact angles, the melt will wick through the pores of the solid, giving rise to *spontaneous impregnation*, whereas for angles larger than $\pi/2$, the sign of the capillary pressure changes and impregnation of the porous solid will be impeded by surface energy effects.

Microscopic inter-particle capillary forces were analysed for two different geometries. The case of two parallel flat solid surfaces bridged by a liquid drop was realised experimentally, confirming the calculation. It was shown that, for small contact angles, the solid surfaces were pulled together due to the wicking of the resin melt, whereas, for angles larger than $\pi/2$, an equilibrium distance between fibres was reached.

Considering the magnitude of the capillary pressure ($\pm 10^4$ Pa), its effects on the impregnation rate can be important for low pressure processing techniques (e.g. vacuum bagging); much care must therefore be taken in the choice of the materials to be used. For processes using higher mechanical pressures ($>10^5$ Pa), the influence of the capillary pressure on the impregnation rate can be neglected, but surface energy effects may determine the content and topology of voids entrapped in the laminate, and thereby affect its mechanical properties.

ACKNOWLEDGEMENT

The authors wish to thank the "Commission pour l'Encouragement à la Recherche Scientifique" (CERS) and Huber+Suhner for the financial support of this investigation. Thanks are also due to Casper Koster who helped carrying out the experimental work, and to Prof. A.G. Gibson for valuable discussions.

REFERENCES

[1] Roychowdhury, S. and S. G. Advani. An Experimental Investigation of Consolidation in Thermoplastic Filament Winding. *Composites Manufacturing*, 2: 97–104, 1991.

[2] Van West, B. P., R. Byron Pipes and S. G. Advani. The Consolidation of Commingled Thermoplastic Fabrics. *Polymer Composites*, 12: 417–427, 1991.

[3] Iyer, S. R. and L. T. Drzal. Manufacture of Powder Impregnated Thermoplastic Composites. *J. Thermoplastic Composite Materials*, 3: 325–355, 1990.

[4] Ahn, K. J., J. C. Seferis and J. C. Berg. Simultaneous Measurements of Permeability and Capillary Pressure of Thermosetting Matrices in Woven Fabric Reinforcement. *Polymer Composites*, 12: 146–152, 1991.

[5] Connor, M., S. Toll, J.-A. E. Månson and A. G. Gibson. A Model for the Consolidation of Aligned Thermoplastic Powder Impregnated Composites. *J. Thermoplastic Composite Materials*, in press, 1994.

[6] Lee, W. I. and G. S. Springer. A Model of the Manufacturing Process of Thermoplastic Matrix Composites. *J. Composite Materials*, 21: 1017–1055, 1987.

[7] Giannotta, G., M. Morra, E. Occhiello, F. Garbassi, L. Nicolais and A. D'Amore. Dynamic Wetting of Carbon Fibers by Viscous Fluids. *J. Colloid and Interface Science*, 148: 571–578, 1992.

[8] Giannotta, G., M. Morra, E. Occhiello, F. Garbassi, L. Nicolais and A. D'Amore. Tensiometric Studies on the Wetting of Carbon Fibres by Viscous Fluids. *Composites Manufacturing*, 3: 59–62, 1992.

[9] Bascom, W. D.and J. B. Romans. Microvoids in Glass-Resin Composites. *Ind. Eng. Chem., Prod. Res. Develop.*, 7: 172–178, 1968.

[10] Kohn E. J., A. G. Sands and R. C. Clark. Quantitative Measurement of Void Content in Glass-Filament-Wound Composites and Correlation of Interlaminar Shear Strength with Void Content. *Ind. Eng. Chem., Prod. Res. Develop.*, 7: 179–183, 1968.

[11] Szymanski, A. *Technical Mineralogy and Petrography*. Elsevier, 1989, p. 593.